About size distribution of particles adsorbed to a spherical whispering-gallery-mode resonator in sensing experiments

VLADIMIR SHUVAYEV,[1] MERI KHURSHUDYAN,[1] AND LEV DEYCH[1,2,*]

[1] *Physics Department, Queens College, Flushing, NY 11367, USA*
[2] *CUNY Graduate Center, 365 5th Ave, New York, NY 10016, USA*
[*] *lev.deych@qc.cuny.edu*

Abstract: Whispering-gallery-mode (WGM) resonators are actively used to sense and size nanoparticles. In a typical experimental setup a WGM resonator is placed in a solution to which particles to be sensed are also added. The size of the particle is inferred from the changes in the spectrum of WGM resonances caused by adsorption of the particle to the resonator's surface. The inference often depends on the assumptions about statistical distribution of the particle sizes. We show in this work that the distribution of sizes of the particles actually detected by the resonator differs from the distribution of sizes in the total population of the particles. This phenomenon, which is currently not being taken into account when interpreting experimental data, might distort sizing information extracted from such experiments.

© 2023 Optica Publishing Group under the terms of the Optica Open Access Publishing Agreement

1. Introduction

Whispering gallery modes (WGM) are excitations of axially symmetrical dielectric optical resonators (cavities) characterized by long lifetimes and high energy density localized in the vicinity of the resonator's surface [1, 2]. They are usually excited by a tapered fiber or a prism and manifest themselves as resonances with very high Q-factors - the values of 10^6 are easily achievable, but Q-factors as high as 10^{11} have been demonstrated [3]. The high Q-factors and the strong concentration of the field of WGM modes in the vicinity of the resonator's surface makes them attractive candidates for sensing applications [4–19]. WGMs are characterized by orbital l, polar m, and radial s quantum numbers defined with respect to a particular coordinate system. So-called fundamental WGMs are distinguished by a single maximum of their intensity distribution with respect to the polar angle θ (see Fig. 1) and in the radial direction. In the coordinate system with equatorial plane defined by the position of this maximum, fundamental WGMs are identified by $m = l$ and $s = 1$. In this work we assume for concreteness that we deal with a fundamental WGM. The field of WGM resonator sensing was pioneered in 2002 paper by Vollmer et al [5], and the single protein detection using WGM resonators was first proposed by Arnold et al in Ref. [4]. The main idea of WGM-based detection mechanism is that a small particle adsorbed on the surface of a resonator will shift (and sometimes split [11, 20–22]) the frequencies of the resonances. The magnitude of the shift (or split) can be used to infer the size of the detected particle. The theoretical foundation for such inference in the "shift" mode was first proposed in Ref. [23] using a perturbation theory, and then extended in the form of the so-called Reactive Sensing Mechanism (RSM) in Ref. [24]. The RSM since then has become an approach of choice for the interpretation of many sensing experiments conducting by different groups [7–10, 17, 25, 26]. An attempt to improve RSM to take into account the finite size of the particles more accurately using an improved perturbation approach was undertaken in Ref. [27].

The splitting regime was first theoretically considered by Mazzei et al in Ref. [20] on the basis of a model involving particle induced interaction between two degenerate counter-propagating WGMs. The interaction removes the degeneracy resulting in two resonance peaks instead of one

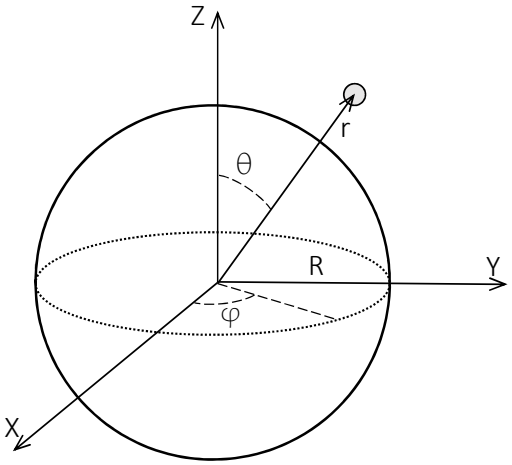

Fig. 1. The spherical coordinate system with an equator defined by the circle of the maximum values of the intensity of the excited mode in the azimuthal and radial directions.

shifted peak. The splitting of WGM resonances has also been used in several papers for sensing and sizing of nanoparticles [11–15, 21, 22].

In Refs. [28, 29] the multi-particle Mie theory in combination with the dipole approximation for the field of the particle was used to develop an *ab initio* theory of interaction between WGMs of a spherical resonator and a nanoparticle, and in Ref. [30] similar approach was applied to the two-dimensional disk resonators. However, comparison with experimental results showed that the spherical approximation cannot be applied to a majority of sensing experiments with nominally spherical resonators because even small (on the order of 1%) deviation from the ideal spherical shape is significant in the context of the interaction with nanoparticles. (The spherical approximation might be applicable to recent experiments with levitating droplet resonators [31], where resonators with a very small deviation from spherical shape were demonstrated.) The theory of Refs. [28, 29] has been extended in Ref. [32] to weakly spheroidal resonators. Results of this work, which provided a justification for the model of the particle-induced coupling between counter-propagating WGMs of Ref. [20] while revealing its limitations, showed a very good agreement with experimental results of Refs. [21, 22]. One of the important results of the *ab initio* approach was demonstration of the emergence of the "shift" regime of the WGM-particle interaction from the splitting regime as a result of the overlap of the split peaks either due to decrease of the particle size or increase of the width of the affected resonances. This phenomenon was more fully investigated in subsequent work, Ref. [33], where the theory of Ref. [32] was applied to the case of ultra-small particles and the process of formation of the single shifted peak from two overlapping split peaks was explicitly demonstrated. These results showed the limits of the RSM empiric formula and allowed to expand its applicability beyond the uniform field approximation on which RSM is based.

In this regard, it needs to be pointed out that the dipole approximation used in Refs. [28,30,32,33] is not equivalent to the uniform field approximation. While the latter requires that $k_0 n_p R_p \ll 1$, where k_0 is the vacuum wave number at the resonance, n_p and R_p are refractive index and the radius of the particle respectively, the former only requires that the contributions from the multipoles with polar number $l > 1$ and the magneto-dipole terms remain smaller than the electro-dipole contribution with $l = 1$. This is a much less stringent requirement and the dipole approximation was shown to remain valid even when $k_0 n_p R_p \sim 1$. Therefore, the results for the

frequency shift derived in Ref. [33] do not require any corrections in the form of a heuristic form factor used in Ref. [10] to extend the validity of RSM beyond the uniform field approximation.

2. Motivation for this work

In the end of Ref. [33] its authors noted that while predictions of that work were in a very good agreement with experimental results of Ref. [6], they deviate by about a factor of 2.5 from data listed in Ref. [10] dealing with larger particles. The situation appeared even more mysterious when it was noticed that the experimental data can be reproduced by replacing the dipole approximation with the uniform field approximation. The problem with such a replacement was, of course, that for the sizes of particles used in Ref. [10] parameter $k_0 n_p R_p \approx 2$ and the uniform field approximation is definitely not valid in this case.

A typical setup of the experiments similar to the one described in Ref. [10] consists in placing a WGM resonator inside a solution containing nanoparticles to be sensed and sized. One (or several) WGM modes are excited in the resonator and once a particle is adsorbed on the resonator's surface, the shift (or splitting) of the spectral line of the resonator is observed. The size of the particle is then inferred from the magnitude of the spectral change using a preferred theoretical model.

There are two fundamental problems that an experimentalist faces in this situation. First, the spectral response of the resonator significantly depends on the landing point of the particle on the resonator's surface - particles landing around the equator, where the field of the excited WGM is the strongest, generate stronger spectral effects than particles landing further away from the equator. At the same time the actual landing point of each particle is not known. The second problem is that to be useful the relation between the spectral effects and the size of the particles must be verified and calibrated using particles of known sizes. However, the exact sizes of adsorbed particles used for calibration/verification are not known. All what is normally known is the mean value and the standard deviation for the ensemble of particles used in the experiment.

The first problem is usually solved by repeating the experiment multiple times and selecting the adsorption event resulting in the largest spectral shift, which allows to assume that this shift was caused by a particle landed in the proximity of the equator. The second problem is "solved" by comparing the particle sizes inferred from the spectral shifts using one's favorite theoretical model with the mean value of the particles in the solution, and if the predicted particle's size lies within one standard deviation from this mean it is declared that the theoretical formula is verified and can be used to determine unknown sizes of the particles. Authors of Ref. [10] suggested an improved solution to the first of these problems based upon using high-order polar WGMs, but its veracity is also based upon the assumption about statistical distribution of particle sizes.

In this work we point out that the tacit assumption that the distribution of sizes of the adsorbed particles is exactly the same as the distribution of the particles placed in the solution is not actually correct. Indeed, the motion of the particles in the aqueous medium is not exactly random and is subjected to the attractive optical force, which significantly increases the likelihood of the adsorption event and decreases the waiting time for it to occur. But it also makes the motion of the particle toward the resonator dependent on its size. In this work we explicitly study the size dependence of the time it takes for a particle to land on the resonator and compare the actual distribution of the sizes of the adsorbed particle with the size distribution in the general population of the particles. Our results show that larger particles reach the resonator faster, and that distribution of the adsorbed particle's sizes is, therefore, skewed toward larger particles.

One can identify two effects responsible for this phenomenon: the dynamical effect arising because the acceleration of the particles, and, hence, the time of travel toward the resonator is size dependent, and geometrical (or kinematic) effect due to the simple fact that larger particles need to travel shorter distance to get adsorbed. Both these effects skew the distribution toward particles with larger sizes, which means that the sizes of particles predicted by RSM are actually

smaller than the average size of the adsorbed particles in agreement with the observation made in Ref. [33]. Apparently, this phenomenon needs to be taken into account when choosing a theoretical model to infer particle sizes from the spectral shifts in the sensing experiments, when the sensed particles are randomly selected by combination of diffusion and optical forcing.

3. Simulation results

3.1. Main assumptions

A full simulation of diffusion of a particle under the action of optical force would require solving the following equation

$$M\frac{d^2\boldsymbol{r}}{dt^2} = \boldsymbol{F}_{opt} - \gamma\boldsymbol{v} + \boldsymbol{\xi}(t), \tag{1}$$

where M is the particle's mass, $\boldsymbol{F}_{opt}$ is the combination of all optical forces, the second term on the r.h.s represents a damping force due to viscosity of the medium, and the last term is the random Langevin force. The random force can be simulated by introducing random changes of particle's momentum distributed according to fluctuation-dissipation theorem, while the motion during some characteristic time $\triangle t$ between the collisions is described by the deterministic version of Eq. 1 with the Langevin term omitted. However, this approach requires significant computational resources while its results depend on the choice of a not very well defined parameter Δt (or even the distribution function of such times). For the modest goals pursued in this work simplified approach appears to be warranted. We chose to ignore the Langevin force altogether, and compute the motion of the particles with randomly chosen initial velocities and initial positions taking into account only the optical and damping forces. Essentially, what we are simulating here is the last step of the particle's motion before it touches the resonator. Strictly speaking, the distribution of particle's velocities in this case is no longer the regular thermal Maxwell distribution, since it has already been affected by the optical force. However, since the optical force decreases rather fast with the distance from the resonator, the deviation of the velocity distribution of particles from Maxwell form shall not be too strong. It would increase the probability of the particle's velocity to be directed toward the resonator rather than away from it, and we can incorporate such a tendency qualitatively by discarding initial velocities with radial components (as defined in the spherical coordinate system centered at the resonator) pointed away from the resonator. To elucidate the effects of such selection we carried out our calculation with and without it.

When calculating the optical force we also neglect the modification of the resonator's optical field due to the presence of the particle. This effect, which was carefully studied in Refs. [34, 35], is significant only at rather small distances between particles and resonator, and does not significantly affect the timing till adsorption, and, hence, our results[1]. Therefore, we compute the optical forces using the standard expression for the force on a polarizable dipole

$$\boldsymbol{F} = \frac{1}{4}Re\left[\alpha\right]\nabla\left|\boldsymbol{E}\left(\boldsymbol{r}\right)\right|^2 + \frac{1}{2}Im\left[\alpha\right]\left(\omega Re\left[\boldsymbol{E}^*(\mathbf{r})\times\boldsymbol{B}(\mathbf{r})\right] + Im\left[\left(\boldsymbol{E}^*(\mathbf{r})\cdot\nabla\right)\boldsymbol{E}(\mathbf{r})\right]\right), \tag{2}$$

where ω is the frequency of the electromagnetic field, $\mathbf{E}$ and $\mathbf{B}$ are complex amplitudes of the electric and magnetic fields in the frequency domain, and α is the complex polarizability of particle of radius R_p with refractive index n_p placed in the medium with refractive index n_m.

[1] It might be significant in the situations when a particle is captured by the resonator's field into an orbital motion around it observed in Ref. [25], but we do not deal with such situations here.

The real and imaginary parts of the polarizability are given by

$$Re\,[\alpha] = 4\pi\varepsilon_0 R_p^3 \frac{n_p^2 - n_m^2}{n_p^2 + 2n_m^2}, \tag{3}$$

$$Im\,[\alpha] = \frac{8\pi\varepsilon_0}{3} k_0^3 R_p^6 \left(\frac{n_p^2 - n_m^2}{n_p^2 + 2n_m^2}\right)^2, \tag{4}$$

where k_0 is the vacuum wave number and ε_0 is the permittivity of vacuum in SI system of units. The term proportional to the real part of the polarizability in Eq. 2 is the so-called gradient force, which is conservative in nature and pushes the particle toward regions with greater field intensity (assuming that $n_p > n_m$), while the term proportional to $Im[\alpha]$ describes the dissipative scattering force. Electric and magnetic fields in Eq. 2 are those of whispering gallery modes excited in the resonator. If the exciting field is tuned exactly to the resonance of one of the resonator's modes, we can assume that $\boldsymbol{E}$ and $\boldsymbol{B}$ are described by corresponding vector spherical harmonics (VSH) [36] - the solutions of vector wave equation in spherical coordinates. Since we assumed that the excited mode is fundamental, we will consider VSHs with $m = l$.

Assuming also that the excited mode is of so-called TE polarization (electric field is everywhere tangential to the surface of the resonator), we present the electric field as

$$\boldsymbol{E}(r,\theta,\varphi) = \boldsymbol{E}_0 \boldsymbol{M}_{l,l}^{(3)}(r,\theta,\varphi), \tag{5}$$

where $\boldsymbol{M}_{l,l}^{(3)}(r,\theta,\varphi)$ is VSHs of TE polarization defined in Ref. [36], and the upper index (3) indicates that the radial dependence of the field is given by Hankel functions. The explicit expressions for the VSH can be found in the Appendix. Substituting Eq. 5 in Eq. 2 (magnetic field is found from the regular Maxwell equation), we present the optical force acting on the particle in the following form

$$\boldsymbol{F}_{opt} = \frac{R_p^3}{R^3} \Lambda(l, n_m, n_p) \left[\boldsymbol{f}^{(gr)}(r,\theta,l) + \frac{R_p^3}{R^3} \boldsymbol{f}^{(sc)}(r,\theta,l)\right]. \tag{6}$$

Parameter $\Lambda(l, n_m, n_p)$, where n_m and n_p are refractive indexes of the medium outside of the resonator and particles, respectively, gives the maximum value of the radial component of gradient part of the optical force corresponding to the radial coordinate of the center of the particle equal to the radius of the resonator R: $r = R$, and the polar angle to the equatorial position: $\theta = \pi/2$. It is defined by the expression:

$$\Lambda(l, n_m, n_p) = \frac{n_m k_0}{2} \varepsilon_0 E_0^2 R^3 \frac{n_p^2 - n_m^2}{n_p^2 + 2n_m^2} \frac{(2l+1)\, l (2l-1)!!}{(l+1)\, 2^l l!} \times \left[j_l(n_m x_r) j_l'(n_m x_r) + y_l(n_m x_r) y_l'(n_m x_r)\right], \tag{7}$$

where $j_l(x)$ and $y_l(x)$ are spherical Bessel functions of the 1st and 2nd kind correspondingly, and the prime indicates differentiation with respect to the entire argument. We also introduced here a dimensionless size parameter x_r defined as $x_r = k_0 R$. Vectors $\boldsymbol{f}^{(gr)}$ and $\boldsymbol{f}^{(sc)}$ in Eq. 6 are dimensionless gradient and scattering forces accordingly dependent on polar angle θ and particle's radial coordinate r. Expressions for components of $\boldsymbol{f}^{(gr)}$ and $\boldsymbol{f}^{(sc)}$ are presented in the Appendix. The important point, which needs to be made now, is that these vectors do not depend upon particle's sizes, so the entire size dependence of the gradient force is given by the factor R_p^3/R^3 in Eq. 6 while the scattering force has an additional R_p^3/R^3 factor making it dependent

on the square of the volume. Assuming that the whispering gallery mode is excited by delivering the optical power P via a fiber of diameter d, Eq. 7 can be rewritten as

$$\Lambda(l, n_m, n_p) = \frac{4P}{c\pi d^2} n_m k_0 R^3 \frac{n_p^2 - n_m^2}{n_p^2 + 2n_m^2} \frac{(2l+1)\, l(2l-1)!!}{(l+1)\, 2^l l!} \times \left[j_l(n_m x_r) j_l'(n_m x_r) + y_l(n_m x_r) y_l'(n_m x_r) \right]. \quad (8)$$

The coefficient γ of the damping force in Eq. 1 is determined by the Stokes law as

$$\gamma = 6\pi\eta R_p, \quad (9)$$

where η is viscosity of the medium containing the particles. Thus, the acceleration of the particles as they move toward the resonator is determined by three factors: acceleration due to gradient optical force is size independent, acceleration due to scattering optical force scales as R_p^3, while the acceleration due to the damping force scales as R_p^{-2}. It seems reasonable to assume, therefore, that the larger particles shall reach the resonator faster resulting in skewing the size distribution of the adsorbed particles toward larger sizes.

3.2. Numerical results for size distribution of the adsorbed particles

It is convenient to rewrite Eq. 1 introducing dimensionless position vector $\boldsymbol{u} = k_0 \boldsymbol{r}$ and dimensionless time $\tilde{t} = t/\tau$, where the time scale τ is defined as

$$\tau = \sqrt{\frac{MR^3}{k_0 R_p^3 \Lambda(l, n_m, n_p)}} = \sqrt{\frac{4\pi\rho_p R^4}{3x_r \Lambda(l, n_m, n_p)}},$$

where ρ_p is the density of the material of the particles (polystyrene) assumed to have a spherical form. Then Eq. 1 can be rewritten in a dimensionless form (omitting the random force)

$$\frac{d^2\boldsymbol{u}}{d\tilde{t}^2} = \boldsymbol{f}^{(gr)}(r, \theta, l) + \frac{R_p^3}{R^3} \boldsymbol{f}^{(sc)}(r, \theta, l) - \frac{\bar{R}_p^2}{R_p^2} \tilde{\gamma} \frac{d\boldsymbol{u}}{d\tilde{t}}. \quad (10)$$

Dimensionless damping parameter $\tilde{\gamma}$ is defined as

$$\tilde{\gamma} = \frac{9\eta\tau}{2\rho_p \bar{R}_p^2}, \quad (11)$$

where we used Stokes law, Eq. 9 and introduce average particle's radius $\bar{R}_p$. It is important to note that the time scale τ does not depend on the particle's size, and, therefore, remains the same for every particle with a randomly generated radius. The dimensionless damping parameter, however, indeed scales as R_p^{-2} weakening the damping force for larger particles.

It is convenient to solve Eq. 11 using representation of all vectors in terms of their spherical components. Writing the position vector $\boldsymbol{u}$ as $\boldsymbol{u} = x\boldsymbol{e}_r$, where $x = k_0 r$ is the dimensionless radial coordinate of the particle, we can rewrite Eq. 11 as the following system

$$\begin{aligned}
\frac{d^2x}{dt^2} - x\left(\frac{d\theta}{dt}\right)^2 \cos^2\varphi - x\left(\frac{d\varphi}{dt}\right)^2 &= f_r^{(gr)} + \frac{R_p^3}{R^3} f_r^{(sc)} - \frac{\bar{R}_p^2}{R_p^2}\tilde{\gamma}\frac{dx}{dt} \\
2\frac{dx}{dt}\frac{d\theta}{dt}\cos\varphi + x\frac{d^2\theta}{dt^2}\cos\varphi - 2x\frac{d\theta}{dt}\frac{d\varphi}{dt}\sin\varphi &= f_\theta^{(gr)} + \frac{R_p^3}{R^3} f_\theta^{(sc)} - \frac{\bar{R}_p^2}{R_p^2}\tilde{\gamma}x\frac{d\theta}{dt}\cos\varphi, \quad (12) \\
2\frac{dx}{dt}\frac{d\varphi}{dt} + x\left(\frac{d\varphi}{dt}\right)^2 \sin\varphi\cos\varphi + x\frac{d^2\varphi}{dt^2} &= f_\varphi^{(gr)} + \frac{R_p^3}{R^3} f_\varphi^{(sc)} - \frac{\bar{R}_p^2}{R_p^2}\tilde{\gamma}x\frac{d\varphi}{dt}
\end{aligned}$$

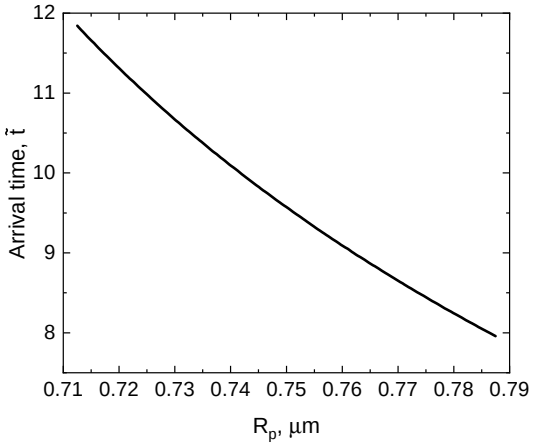

Fig. 2. Dependence of the time to adsorption upon particle's radius for the same initial conditions.

where sub-indexes r, θ, φ refer to the corresponding components of the respective vectors.

The experiments that we intend to simulate, use whispering gallery modes with large orbital numbers $l \sim 700$. In our calculations we use much smaller $l = 40$, which doesn't affect the main conclusions of the work while significantly simplifying computation of Bessel functions. However, in order to maintain a realistic balance between optical and damping forces, we have to adjust the value of viscosity η to compensate for the significantly decreased magnitude of the optical forces at smaller l. To find the appropriate value of η we first compute "characteristic" damping force defined as

$$f_l^{(damp)} = \tilde{\gamma} v_{rst},$$

where v_{rst} is dimensionless root-mean-square force of particles in the solution:

$$v_{rst} = \sqrt{\frac{2k_B T x_r}{3\pi \Lambda(l, n_m, n_p)} \frac{R^2}{\bar{R}_p^3}},$$

where k_B is the Boltzmann constant, for $l = 720$ and the corresponding value of the size parameter x_r using the actual value of the viscosity of water at room temperature. Then we repeat these calculations for $l = 40$, and choose the adjusted value of the viscosity to ensure that $f_{720}^{(damp)} = f_{40}^{(damp)}$. The goal of our simulations is to establish the distribution of the sizes of the particles which first reach the surface of the resonator. To this end we generate an ensemble of 100 particles, compute the time until the radial coordinate of the particle becomes $x \leq x_r + k_0 R_p$, and record the size of the particle that takes the least time to "touch" the surface of the resonator, and the angular coordinates of the "adsorption" site. We repeat these calculations 10,000 times and built the histogram showing the size distribution of the adsorbed particles. The sizes of the particles in the original distribution are chosen randomly from a uniform distribution with mean $\bar{R}_p = 0.75\mu m$ and standard deviation $\sigma_p = 0.0375\mu m$, and the particles are placed at randomly chosen initial positions within a spherical ring surrounding the resonator. The radius of the resonator in these calculations was chosen to be $56\mu m$, which is given only for comparison with the sizes of adsorbed nanoparticles. The only essential characteristic of the resonator, which is needed for the calculations, is the size parameter x_r. To elucidate the effect of the choice of the region of the initial positions on the results of our simulations, we carried out our calculations with three different regions defined by the radius of their inner and outer spherical surfaces. Using dimensionless radial coordinate these three regions are

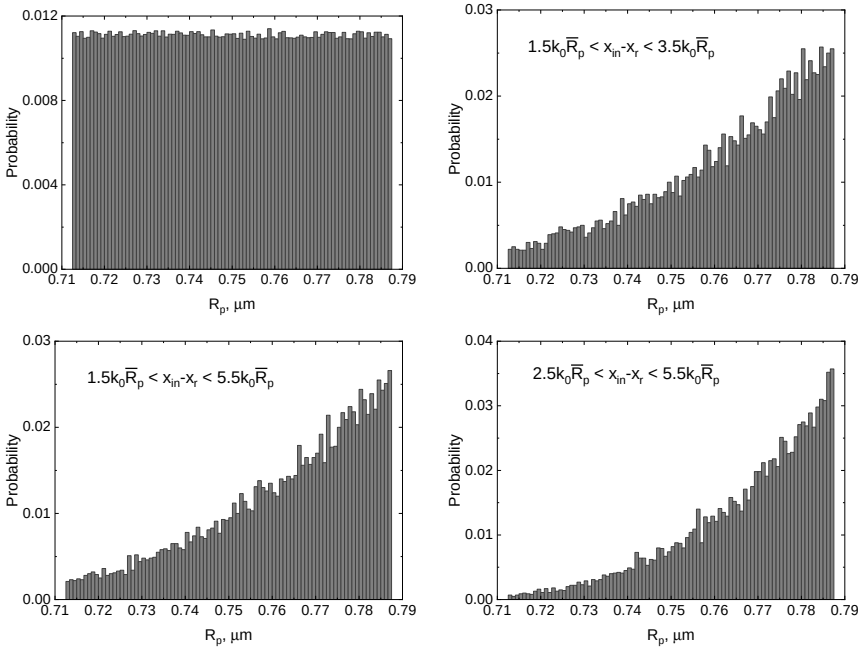

Fig. 3. First row left: uniform size distribution of the generated random ensemble of the particles. The rest of graphs show the size distribution of the particles that were first adsorbed to the resonator's surface with initial positions drawn from three different regions.

defined as: $x_r + 1.5k_0\bar{R}_p < x_{in} < x_r + 3.5k_0\bar{R}_p$, $x_r + 1.5k_0\bar{R}_p < x_{in} < x_r + 5.5k_0\bar{R}_p$, and $x_r + 2.5k_0\bar{R}_p < x_{in} < x_r + 5.5k_0\bar{R}_p$, where x_{in} is the dimensionless radial coordinate of the initial position of a particle, and $\bar{R}_p$ is the mean value of particle's radiuses. The initial velocities of the particles are chosen from Maxwell distribution corresponding to the room temperature. To estimate the significance of the effect of the possible deviation in the velocity distribution from Maxwell form due to optical forcing during the preceding steps of particle's motion, mentioned in Section 1, we carried our the calculations with and without rejection of the initial velocities directed away from the resonator. The refractive indexes of the particles and of the aqueous medium were chosen to be $n_p = 1.572$, and $n_m = 1.326$ respectively.

We begin presenting our results with Fig. 2, which depicts the dependence of the time it takes a particle to reach the surface of the resonator upon its radius for particles with same initial position and the same initial velocity. This calculation confirms the assumption that particles with larger diameters reach the resonator faster. To illustrate that this effect is indeed results in skewing the size distribution of the adsorbed particles we present Fig. 3, which shows the histograms of particle's sizes that were the first to reach the resonator for three different initial regions together with the distribution of the particle's sizes in the solution. Two main conclusions can be drawn from these graphs. First, the actual size distribution of the adsorbed particles is strongly skewed toward particles of larger sizes compared to the uniform distribution for the general population of the particles in the solution, and second, the skewing phenomenon persists for all studied regions of particles' initial positions. One can conclude, therefore, that the deviation of the distribution from uniform is likely a real and general phenomenon, which, of course, is also confirmed by the size dependence of the particles' travel time (Fig. 2).

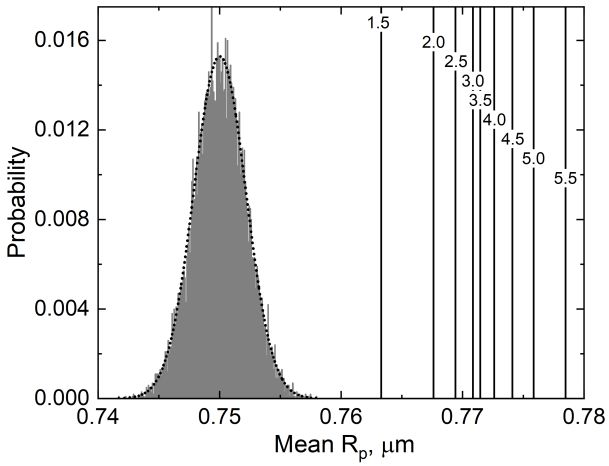

Fig. 4. Distribution of the mean sizes in the sample of 100 particles drawn from a uniform distribution. The dotted line is a fit of the empirical distribution by a Gaussian function, and the vertical lines correspond to the mean radii of the first to get adsorbed particles in each sample for different regions of the initial particles' coordinates.

In order to further quantify and verify the statistical significance of the deviation of the observed histogram from the uniform distribution, we run statistical test using the assumption of the uniform distribution as a null-hypothesis and the mean size as a test statistics. If the distribution of the particle sizes were uniform, the distribution of the averages sizes in 10,000 batches of 100 particle ensembles would have to obey the Bates distribution, which for the large sample size is close to normal. We constructed the distribution of the mean sizes in our ensemble of 10,000 means computed for the groups of 100 particles, which is indeed resemble the expected normal distribution and compared it with the mean sizes of the particles landed on the resonator for several regions of particle's initial coordinates. (Fig. 4). The latter are presented by vertical lines, and the numbers next to these lines signify the lower boundary of the region of the initial positions of the particles in terms of their mean radius (the thickness of the spherical layer in cases was equal to $2k_0\bar{R}_p$). For all initial regions the mean sizes of the adsorbed particles lie so far at the tail of the Bates distribution that we were unable to estimate the p-value of the test using the histogram of the averages - there were simply no available average values in the simulated ensemble. One can also notice that with increase of the region of the initial positions, the average size of the adsorbed particles is moving further to the right. This phenomenon can be understood by noting that the travel time to the surface of the resonator decreases with increasing size of the particle (see Fig. 2), so that the farther the initial position of a particle is the more likely it is for a larger particle to arrive earlier. These results allows us to reject the null hypothesis with great confidence and conclude that the distribution of the sizes of the adsorbed particles is strongly skewed toward larger sizes, so that the average size of the adsorbed particles is significantly larger than the average of the particles in the solution.

As a byproduct of our simulations we recorded the angular (θ) coordinate of the landing points of the adsorbed particles. The distributions of this angular coordinate for different regions of particle's initial positions are shown in Fig. 5. The plots in the first row show expected bell-shaped distribution of the landing points corresponding to the Gaussian angular distribution of the intensity of the field of a fundamental WGM. However, the graph in the second row of this figure revealed an unexpected phenomenon - a bimodal distribution of the landing coordinates for particles with initial coordinates farther away from the resonator. This phenomenon reflects

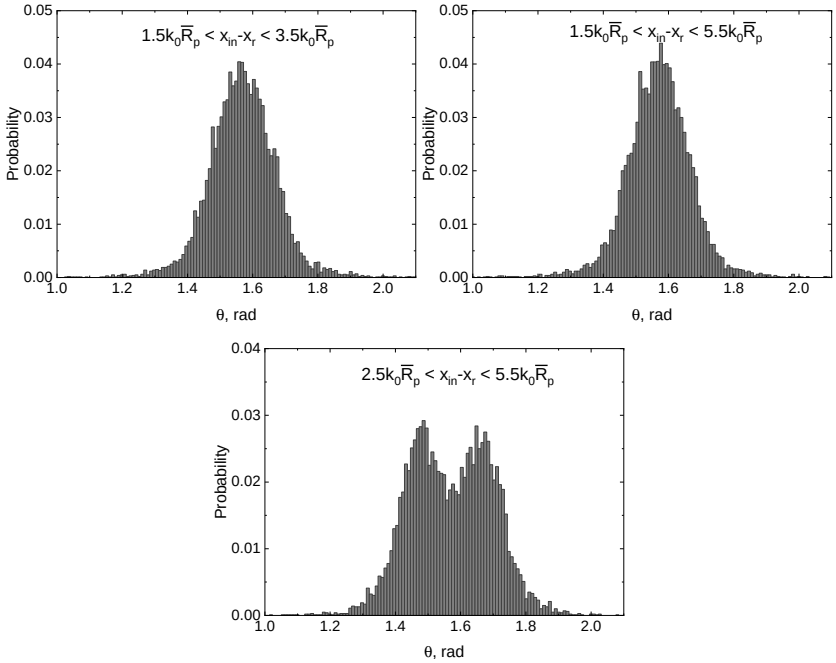

Fig. 5. The distributions of the landing angles for different regions of the initial positions: first raw corresponds to initial radial coordinates lying between $1.5k_0\bar{R}_p$ and $3.5k_0\bar{R}_p$ (left) and $1.5k_0\bar{R}_p$ and $5.5k_0\bar{R}_p$ (right). The graph in the second raw corresponds to the initial positions between $2.5k_0\bar{R}_p$ and $5.5k_0\bar{R}_p$

the increased role of the scattering optical force for remote particles, which is not governed by the maximum of the intensity of the field.

4. Conclusion

In this work we simulated typical sensing experiments, in which the size of the particle adsorbed to a resonator's surface from a solution is determined based on the shift (or splitting) of a spectral line of a whispering-gallery-mode resonator. Our simulations demonstrate that the main assumption used for interpretation of the results of such experiments, namely that the size distribution of the adsorbed particles is the same as the initial size distribution of the particles in the solution, is incorrect. We found that the particles with larger diameters are more likely to reach the resonator first, and, therefore, the size distribution of the adsorbed particles is skewed toward larger sizes. This effect needs to be taken into account when validating theoretical models used to infer particle's size from the spectral shifts. In particular, this effect might explain the results of Ref. [33], which predicted particle sizes larger than the average size of the particles used in experiment of Ref. [10].

Appendix

Vector Spherical Harmonics

In this work we follow the definition of Vector Spherical Harmonics $\boldsymbol{M}^{(3)}_{m,l}(r,\theta,\varphi)$ presented in Ref. [36]:

$$\boldsymbol{M}^{(3)}_{m,l}(r,\theta,\varphi) = \gamma_{m,l}\boldsymbol{C}_{m,l}(\theta,\varphi)\, h^{(1)}_l(kr),$$

where

$$\gamma_{m,l} = \sqrt{\frac{(2l+1)(l-m)!}{4\pi l(l+1)(l+m)!}},$$

$$\boldsymbol{C}_{m,l}(\theta,\varphi) = \left[\boldsymbol{e}_\theta \frac{im}{\sin\theta} P_l^m(\cos\theta) - \boldsymbol{e}_\varphi \frac{d}{d\theta} P_l^m(\cos\theta)\right] e^{im\varphi},$$

and $h_l^{(1)}(kr)$ is the spherical Hankel function of the 1st kind. This spherical harmonic describes an electric field of TE polarization (no radial component). $\boldsymbol{e}_\theta$ and $\boldsymbol{e}_\varphi$ are unit vectors of the spherical coordinate system representing azimuthal and polar directions correspondingly. The spherical harmonics $\boldsymbol{N}_{m,l}(r,\theta,\varphi)$ that describe the electric field of TM polarization (in this case the magnetic field has no radial component) are defined as $\boldsymbol{N}_{m,l}(r,\theta,\varphi) = \nabla \times \boldsymbol{M}_{m,l}(r,\theta,\varphi)/k$, but we did not use these VSHs in our calculations.

Optical forces

Here we provide readers with expressions for the different components of the optical force used in our simulations. This force can be divided into the gradient and scattering parts, the first being conservative, and the second dissipative. The spherical components of the gradient force are given as:

radial:

$$f_r^{(gr)} = \sin^{2l-2}\theta\left(1+\cos^2\theta\right)\frac{j_l(n_m x)j_l'(n_m x) + y_l(n_m x)y_l'(n_m x)}{j_l(n_m x_r)j_l'(n_m x_r) + y_l(n_m x_r)y_l'(n_m x_r)} \tag{13}$$

azimuthal :

$$f_\theta^{(gr)} = \sin^{2l-3}\theta\left((l-1)\left(1+\cos^2\theta\right) - \sin^2\theta\cos\theta\right)\times \frac{j_l^2(n_m x) + y_l^2(n_m x)}{n_m x\left[j_l(n_m x_r)j_l'(n_m x_r) + y_l(n_m x_r)y_l'(n_m x_r)\right]} \tag{14}$$

The polar (φ) component of the gradient force is zero. The scattering part of the optical force has only radial and polar components given as follows:

radial:

$$f_r^{(sc)} = \frac{2}{3}n_m\frac{x_r^3}{x^2}\frac{R_p^3}{R^3}\frac{n_p^2-n_m^2}{n_p^2+2n_m^2}\sin^{2l-2}\theta\left(1+\cos^2\theta\right)\frac{1}{j_l(n_m x_r)j_l'(n_m x_r) + y_l(n_m x_r)y_l'(n_m x_r)} \tag{15}$$

polar:

$$f_\varphi^{(sc)} = \frac{2}{3}n_m^2\frac{x_r^3}{x}\frac{R_p^3}{R^3}\frac{n_p^2-n_m^2}{n_p^2+2n_m^2}\sin^{2l-3}\theta\frac{\{l(1+\sin\theta)-\cos 2\theta\}\left(j_l^2(n_m x) + y_l^2(n_m x)\right)}{j_l(n_m x_r)j_l'(n_m x_r) + y_l(n_m x_r)y_l'(n_m x_r)} \tag{16}$$

Funding. Content in the funding section will be generated entirely from details submitted to Prism. Authors may add placeholder text in the manuscript to assess length, but any text added to this section in the manuscript will be replaced during production and will display official funder names along with any grant numbers provided. If additional details about a funder are required, they may be added to the Acknowledgments, even if this duplicates information in the funding section. See the example below in Acknowledgements.

Disclosures. "The authors declare no conflicts of interest."

Data availability. Data underlying the results presented in this paper are not publicly available at this time but may be obtained from the authors upon reasonable request.

References

1. A. B. Matsko and V. S. Ilchenko, Optical resonators with whispering-gallery modes-part i: basics, IEEE J. Sel. Top. Quantum Electron. **12**, 3–14 (2006).
2. V. S. Ilchenko and A. B. Matsko, Optical resonators with whispering-gallery modes-part ii: applications, IEEE J. Sel. Top. Quantum Electron. **12**, 15–32 (2006).
3. A. A. Savchenkov, A. B. Matsko, V. S. Ilchenko, and L. Maleki, Optical resonators with ten million finesse, Opt. Express **15**, 6768 (2007).
4. S. Arnold, M. Khoshsima, I. Teraoka, S. Holler, and F. Vollmer, Shift of whispering-gallery modes in microspheres by protein adsorption, Opt. Lett. **28**, 272 (2003).
5. F. Vollmer, D. Braun, A. Libchaber, M. Khoshsima, I. Teraoka, and S. Arnold, Protein detection by optical shift of a resonant microcavity, Appl. Phys. Lett. **80**, 4057–4059 (2002).
6. S. I. Shopova, R. Rajmangal, Y. Nishida, and S. Arnold, Ultrasensitive nanoparticle detection using a portable whispering gallery mode biosensor driven by a periodically poled lithium-niobate frequency doubled distributed feedback laser, Rev. Sci. Instruments **81**, 103110 (2010).
7. S. I. Shopova, R. Rajmangal, S. Holler, and S. Arnold, Plasmonic enhancement of a whispering-gallery-mode biosensor for single nanoparticle detection in aqueous solution, Appl. Phys. Lett. **98**, 243104 (2011).
8. V. R. Dantham, S. Holler, V. Kolchenko, Z. Wan, and S. Arnold, Taking whispering gallery-mode single virus detection and sizing to the limit, Appl. Phys. Lett. **101**, 043704 (2012).
9. V. R. Dantham, S. Holler, C. Barbre, D. Keng, V. Kolchenko, and S. Arnold, Label-free detection of single protein using a nanoplasmonic-photonic hybrid microcavity, Nano Lett. **13**, 3347–3351 (2013).
10. D. Keng, X. Tan, and S. Arnold, Whispering gallery micro-global positioning system for nanoparticle sizing in real time, Appl. Phys. Lett. **105**, 071105 (2014).
11. J. Zhu, S. K. Ozdemir, Y.-F. Xiao, L. Li, L. He, D.-R. Chen, and L. Yang, On-chip single nanoparticle detection and sizing by mode splitting in an ultrahigh-q microresonator, Nat. Photonics **4**, 46–49 (2010).
12. J. Zhu, Şahin Kaya Özdemir, L. He, D.-R. Chen, and L. Yang, Single virus and nanoparticle size spectrometry by whispering-gallery-mode microcavities, Opt. Express **19**, 16195 (2011).
13. Şahin Kaya Özdemir, J. Zhu, X. Yang, B. Peng, H. Yilmaz, L. He, F. Monifi, S. H. Huang, G. L. Long, and L. Yang, Highly sensitive detection of nanoparticles with a self-referenced and self-heterodyned whispering-gallery raman microlaser, Proc. National Acad. Sci. United States Am. **111**, E3836–E3844 (2014).
14. L. He, Şahin Kaya Özdemir, J. Zhu, W. Kim, and L. Yang, Detecting single viruses and nanoparticles using whispering gallery microlasers, Nat. Nanotechnol. **6**, 428–432 (2011).
15. L. He, Şahin Kaya Özdemir, J. Zhu, and L. Yang, Ultrasensitive detection of mode splitting in active optical microcavities, Phys. Rev. A **82**, 053810 (2010).
16. Y. Shen and J.-T. Shen, Nanoparticle sensing using whispering-gallery-mode resonators: Plasmonic and rayleigh scatterers, Phys. Rev. A **85**, 013801 (2012).
17. T. Lu, H. Lee, T. Chen, S. Herchak, J.-H. Kim, S. E. Fraser, R. C. Flagan, and K. Vahala, High sensitivity nanoparticle detection using optical microcavities, Proc. National Acad. Sci. USA **108**, 5976–5979 (2011).
18. J. D. Swaim, J. Knittel, and W. P. Bowen, Detection limits in whispering gallery biosensors with plasmonic enhancement, Appl. Phys. Lett. **99**, 243109 (2011).
19. J. Knittel, T. G. McRae, K. H. Lee, and W. P. Bowen, Interferometric detection of mode splitting for whispering gallery mode biosensors, Appl. Phys. Lett. **97**, 123704 (2010).
20. A. Mazzei, S. Götzinger, L. de S. Menezes, G. Zumofen, O. Benson, and V. Sandoghdar, Controlled coupling of counterpropagating whispering-gallery modes by a single rayleigh scatterer: A classical problem in a quantum optical light, Phys. Rev. Lett. **99**, 173603 (2007).
21. W. Kim, Şahin Kaya Özdemir, J. Zhu, L. He, and L. Yang, Demonstration of mode splitting in an optical microcavity in aqueous environment, Appl. Phys. Lett. **97**, 071111 (2010).
22. W. Kim, Şahin Kaya Özdemir, J. Zhu, and L. Yang, Observation and characterization of mode splitting in microsphere resonators in aquatic environment, Appl. Phys. Lett. **98**, 141106 (2011).
23. I. Teraoka, S. Arnold, and F. Vollmer, Perturbation approach to resonance shifts of whispering-gallery modes in a dielectric microsphere as a probe of a surrounding medium, J. Opt. Soc. Am. B **20**, 1937 (2003).
24. F. Vollmer, S. Arnold, and D. Keng, Single virus detection from the reactive shift of a whispering-gallery mode, PNAS **105**, 20701–20704 (2008).
25. S. Arnold, D. Keng, S. I. Shopova, S. Holler, W. Zurawsky, and F. Vollmer, Whispering gallery mode carousel - a photonic mechanism for enhanced nanoparticle detection in biosensing, Opt. Express **17**, 6230 (2009).
26. S. Arnold, S. I. Shopova, and S. Holler, Whispering gallery mode bio-sensor for label-free detection of single molecules: thermo-optic vs reactive mechanism, Opt. Express **18**, 281 (2010).
27. M. R. Foreman, D. Keng, E. Treasurer, J. R. Lopez, and S. Arnold, Whispering gallery mode single nanoparticle detection and sizing: the validity of the dipole approximation, Opt. Lett. **42**, 963 (2017).
28. L. Deych and J. Rubin, Rayleigh scattering of whispering gallery modes of microspheres due to a single dipole scatterer, Phys. Rev. A **80**, 061805 (2009).
29. J. T. Rubin and L. Deych, Ab initio theory of defect scattering in spherical whispering-gallery-mode resonators, Phys. Rev. A **81**, 053827 (2010).
30. L. Deych, M. Ostrowski, and Y. Yi, Defect-induced whispering-gallery-mode resonances in optical microdisk

resonators, Opt. Lett. **36**, 3154 (2011).
31. J. Kher-Alden, S. Maayani, L. L. Martin, M. Douvidzon, L. Deych, and T. Carmon, Microspheres with atomic-scale tolerances generate hyper-degeneracy, Phys. Rev. X **10**, 031049 (2020).
32. L. Deych and V. Shuvayev,Theory of nanoparticle-induced frequency shifts of whispering-gallery-mode resonances in spheroidal optical resonators, Phys. Rev. A **92**, 013842 (2015).
33. L. Deych and V. Shuvayev, Spectral modification of whispering-gallery-mode resonances in spheroidal resonators due to interaction with ultra-small particles, Opt. Lett. **40**, 4536 (2015).
34. J. T. Rubin and L. Deych, On optical forces in spherical whispering gallery mode resonators, Opt. Express **19**, 22337 (2011).
35. J. T. Rubin and L. I. Deych, Optical forces due to spherical microresonators and their manifestation in optically induced orbital motion of nanoparticles, Phys. Rev. A **84**, 023844 (2011).
36. M. Mishchenko, L. Travis, and A. Lacis, *Scattering, Absorption, and Emission of Light by Small Particles* (Cambridge University Press, 2002).